OXFORD

ELEMENTS OF A SUSTAINABLE WORLD

John Evans

ELEMENTS OF A SUSTAINABLE WORLD

Elements of a Sustainable World

John Evans

University of Southampton

OXFORD
UNIVERSITY PRESS

OXFORD
UNIVERSITY PRESS

Great Clarendon Street, Oxford, OX2 6DP,
United Kingdom

Oxford University Press is a department of the University of Oxford.
It furthers the University's objective of excellence in research, scholarship,
and education by publishing worldwide. Oxford is a registered trade mark of
Oxford University Press in the UK and in certain other countries

First Edition published in 2020

Impression: 1

Published in the United States of America by Oxford University Press
198 Madison Avenue, New York, NY 10016, United States of America

British Library Cataloguing in Publication Data
Data available

Library of Congress Control Number: 2019954843

ISBN 978–0–19–882783–2 (Hbk.)
ISBN 978–0–19–882784–9 (Pbk.)

DOI: 10.1093/oso/9780198827832.001.0001

Printed and bound by
CPI Group (UK) Ltd, Croydon, CR0 4YY

Preface

We now have 118 known chemical elements as our palette in our context of sustaining our world. Whatever patterns we would like to paint with the elements, we are influenced by the pressures that we all are exerting on spaceship Earth and its inhabitants of all species. In this book our context is considered in terms of the four spheres of the ancient world: Earth, Air, Fire and Water. This book shows how chemical principles can be used to understand the pressures on our world spanning from greenhouse emissions through freshwater supplies to energy generation and storage. The supply of the chemical elements is key to their contribution to alleviating these pressures. Most synthetic and radioactive elements are not available in sufficient supply to contribute in this. Some solutions, such as wind turbines, batteries, fuel cells and automotive exhaust remediation pose questions about sustainable supplies of critical elements. With an eye on the target of the IPCC of capping the temperature anomaly to 1.5 ^{o}C (RCP2.6), options for carbon capture and storage, and the generation of energy and element supply from the sea are assessed. The consequences of the escape of plastics and pharmaceuticals into the wider environment for water integrity are also considered. The final chapter assesses the prospects for planet Earth as viewed in 2019. I have included questions at the end of each chapter. If we consider the elements of learning of learning as being knowledge, understanding, application and evaluation, the bulk of the questions are on a combination of knowing something and understanding it well enough to tackle a new situation. There are no "write what you know about" questions.

This book is a substantial amplification of the 12-lecture slot half unit so that it could provide a course book for a full semester unit. It is based upon students having experience of undergraduate chemistry to the second year. In principle, sections could be extracted for use from year 2, through graduating years to Masters level, depending on the experience of the cohort. The aim has been to marry chemical principles and environmental context. For those mainly experienced in chemical principles, it should provide routes to understand environmental consequences and the demands of sustainability using concepts like embodied energy, carbon and water. For those coming to the topic with a strong interest in sustainability it will provide a chemical basis for the causes of environmental impact and also guidelines for technologies and lifestyles that should be sustainable.

Acknowledgements

The thoughtline to this book began at the Royal Society Theo Murphy Symposium held in July 2010 entitled The sustainable planet: opportunities and challenges for science, technology and society.[1] I am grateful to Judith Howard and Martyn Chamberlain for organising this far-reaching and inspirational symposium. As a result, we initiated a new course in Sustainable Chemistry at Southampton, and I wish to thank Robert Raja for his encouragement in that. I am grateful that Sonke Adlung at OUP saw merit in the proposal that I submitted to him in 2017, and to the Press for agreeing to accept a submission.

Over the last two years this has figured largely for me. I am very grateful for friends and colleagues for their advice and support. Particularly, I am grateful to Phil Gale, Gill Reid, Bill Levason, David Read and Peter Wells at Southampton. In and around Romsey, the support from friends at RMC has been very important to me. The writing has impacted most on my family. Beccy and Simon, and Lisa and Ed and, of course, Hilary have been the bedrock. I know so many things that I have not been able to do over the last two years when Hilary has herself given much time to her own roles. Now I should care for our expended carbon budget and paint the house!

John Evans, 4 November 2019

[1] Ed. J. A. K. Howard, M. Chamberlain, The sustainable planet: opportunities and challenges for science, technology and society, *Phil. Trans. R. Soc A*, 2011, **369**, 1713–1882.

Bibliography

This bibliography comprises a list of some key books and reports that were very in influential in writing this book.

D. J. C. MacKay, *Sustainable Energy - without the hot air*, UIT Cambridge, Cambridge, UK, 2009.

J. M. Allwood, J. M. Cullen, *Sustainable Materials with both eyes open*, UIT Cambridge, Cambridge, 2012.

M. F. Ashby, *Materials and the Environment*, Second Edition, Butterworth-Heinemann, Oxford, 2013.

J. T. Houghton, *Global Warming. The Complete Briefing*, Fifth Edition, Cambridge University Press, 2015.

M. F. Ashby, *Materials and the Environment*, Butterworth-Heinemann, Elsevier, Oxford, 2nd. ed., 2018.

Global Warming of 1.5 °C IPCC report SR15, 2018, https://www.ipcc.ch/sr15/

USGS National Minerals Information Center, Commodity Summaries, 2019.

Contents

Planet Earth

1

1.1 Planetary Resources

For some years, the WWF organization has published some quantitative assessments of the use of our planet.[1] Fig. 1.1 shows the estimates for the total **ecological footprint** of humanity on this world, and its subdivision into different classes of use.[2,3] The area of global hectare area (the biocapacity of the world) is not a constant, and this value increases with the biological productivity. In 1961 world biocapacity was estimated to be 9.5 Gha, clearly in excess of the ecological footprint for that year. Increases in productivity through to 2013 raised biocapacity to 12.2 Gha, considerably in deficit with the ecological footprint. Recognizing that there is some margin for error in these figures, the pattern is still clear. Overall, the total pressure on our world has increased very markedly over the past 50 years (by a factor of *c.*4) (Fig. 1.1).

To some measure this might be linked to the change in human population through that time (Fig. 1.2), but the estimated increase in our ecological footprint also suggests there is an increase in the per capita footprint. As the expansion in the figure shows, population has essentially doubled between 1970 and 2020.

However, this need not be an inexorable trend. Public health and educational opportunities can change this pattern to a considerable extent. As life expectancy increases beyond 50 there is a general trend across most countries in the world for the fertility rate to decline. Indeed, the fertility rate has halved over the last 50 years (Fig 1.3) and is now approaching 2.4.[4] In time, this would help stabilize population levels.

1.2 Differential Pressure on Land, Freshwater, and Oceans

The effects of humanity on the components of the world's systems have varied considerably (Fig. 1.1). The overall load on the planet has not increased as rapidly as population. Indeed the meat- and fish-supplying space (fishing and grazing) showed relatively small changes, but cropland a significant rise. This may be a combination of change of land use, increased efficiency, and overuse. However,

[1] http://wwf.panda.org.

[2] http://data.footprintnetwork.org/.

[3] The ecological footprint is defined as the biologically productive area that is needed to provide everything that people use.

[4] Data from the World Bank, http://data.worldbank.org/indicator.

Elements of a Sustainable World. John Evans, Oxford University Press (2020). © John Evans.
DOI: 10.1093/oso/9780198827832.003.0001

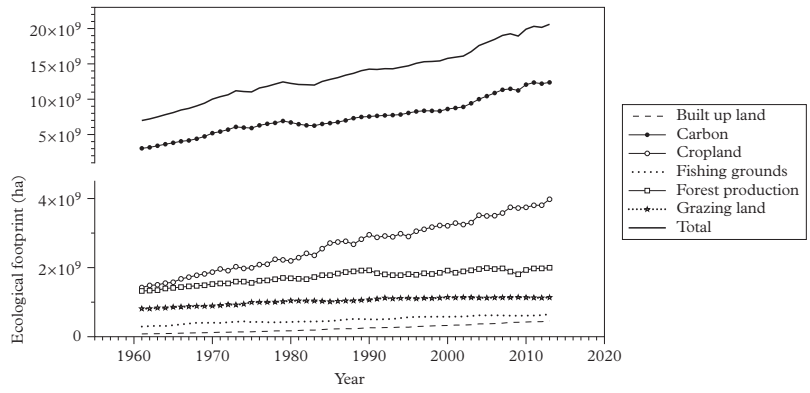

Figure 1.1 *Estimated world ecological footprint (hectares) by land type from 1961 to 2013.*

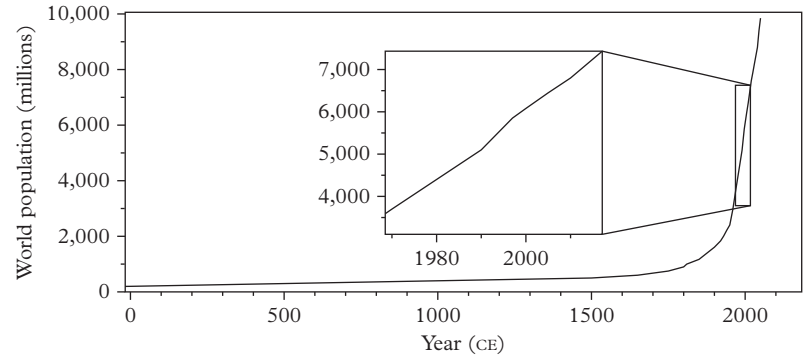

Figure 1.2 *World population from the start of the Christian era (CE) to that estimated for 2050.*

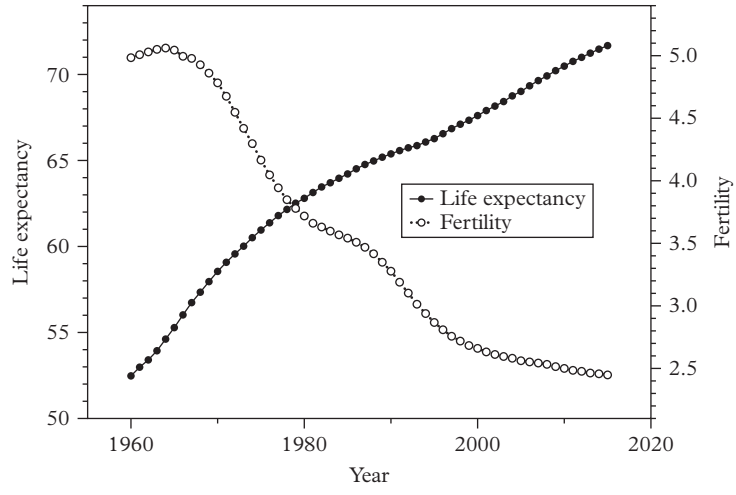

Figure 1.3 *World life expectancies and lifetime fertility rates from 1960 to 2015.*

the dominant change is in the carbon- related part of the system, and that is largely due to energy use.[5] Not surprisingly, a strong theme in this book will be to address carbon- and energy-related factors.

[5] The carbon footprint is represented by the area of forest land required to sequester the CO_2 emissions from fossil fuel use.

1.3 Effects of CO_2 Increases

Over a similar time frame, the mean annual concentration of atmospheric CO_2 has shown an increase of *c.*25% with an upward sloping curve (Fig. 1.4).[6] This curve has been extended backwards using the record of atmospheric composition frozen in ice cores (Fig. 1.5).[7] That shows that the trend has been rising since the 1700s from a value of 280 ppm (molecules of $CO_2/10^6$ molecules of air), taken as the pre-industrial level. Exceeding a value of 300 ppm in the 1900s can be seen as a significant departure from the patterns derived from analysis of ice cores dated over the past 800,000 years (Fig. 1.6).[8]

In the main, the sources of atmospheric CO_2 attributable to the burning of fossil fuels can be tracked by production and sales records. From a starting level

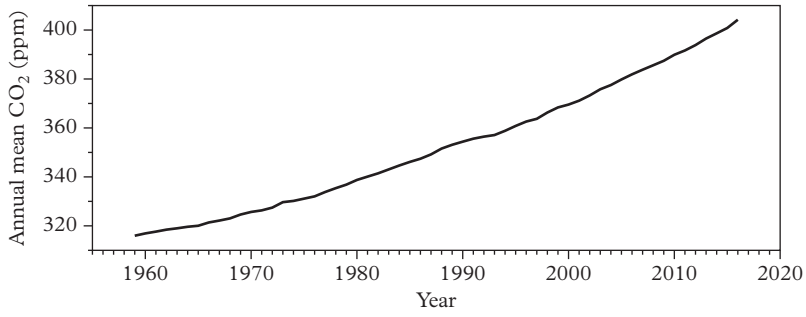

Figure 1.4 *Mean annual concentrations of atmospheric CO_2 measured at the Mauna Loa Observatory, Hawaii, since 1959.*

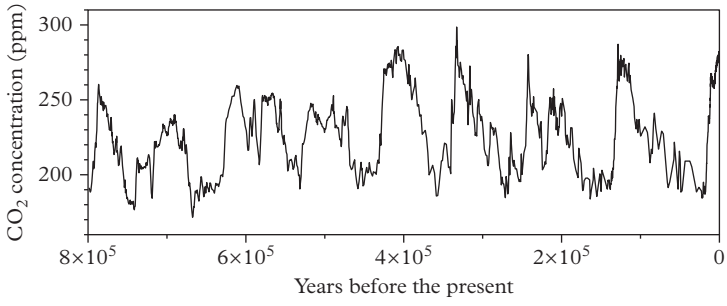

Figure 1.6 *Record of atmospheric CO_2 from ice cores over the past 800,000 years.*

[6] P. Tans, NOAA/ESRL and R. Keeling, Scripps Institution of Oceanography (http://scrippsco2.ucsd.edu/) (http://www.esrl.noaa.gov/gmd/ccgg/trends/).

[7] D. M. Etheridge, L. P. Steele, R. L. Langenfelds, R. J. Francey, Division of Atmospheric Research, CSIRO, Victoria, Australia; J.-M. Barnola, Laboratoire de Glaciologie et Geophysique de l'Environnement, Saint Martin d'Heres, France; V. I. Morgan, Antarctic CRC and Australian Antarctic Division, Hobart, Tasmania, Australia.

[8] D. Lüthi, M. Le Floch, B. Bereiter, T. Blunier, J.-M. Barnola, U. Siegenthaler, D. Raynaud, J. Jouzel, H. Fischer, K. Kawamura, and T. F. Stocker. 'High-resolution carbon dioxide concentration record 650,000–800,000 years before present'. *Nature*, 2008, **453**, 379–82.

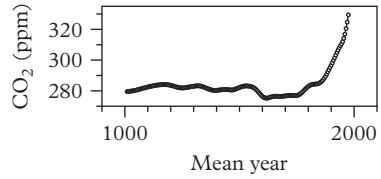

Figure 1.5 *Historical record of atmospheric CO_2 from 75 year averages from ice cores.*

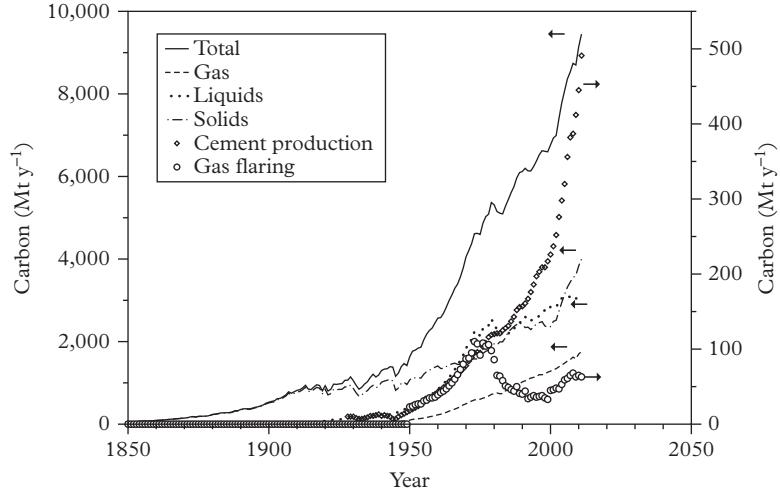

Figure 1.7 *Carbon from fossil fuels burnt annually since 1850.*

of *c.*3 Mton y^{-1} in 1751 there was a rise to 8 Mton y^{-1} by 1800 and 50 Mton y^{-1} in 1849; all of this was by the burning of solid fuel.[9] Post 1850, overall use increased substantially and diversified in terms of source and use (Fig. 1.7). Burning of liquid fuels commenced in 1870, but solid fuel predominated until after 1950. The two sources have been largely comparable in their use since 1970, although there has been a significant increase in solid-fuel consumption since 2000. The burning of natural gas was at a low level until 1950, and even by 2011 its use in terms of carbon was about half that of solid and of liquid fuels. The flaring of natural gas peaked at just over 100 Mton y^{-1} in the 1970s (out of a total of *c.*9450 Mton y^{-1}) and has fallen since. The largest source of industrially related production that burns fossil fuels is cement production. This tracked with gas-flaring until the late 1970s, and since then has continued to rise, nearing 500 Mton y^{-1} in 2011, 5% of the total.

These changes in atmospheric CO_2 concentration have been accompanied by other observations that might be expected to be correlated with it. The ability of atmospheric gases to absorb energy and thus increase the temperature of the atmosphere was proposed in the early 1900s by Joseph Fourier and Claude Pouillet. John Tyndall measured the absorption properties of specific gases, notably water vapour and CO_2.[10] These effects were modelled by Svante Arrhenius, who considered the consequence of the burning of coal, the prime fossil fuel of that time.[11] His conclusions included a prediction of a temperature rise of 8–9 °C in the Arctic regions if the level of CO_2 increased by a factor of

[9] T. Boden and B. Andres, 'Global CO_2 emissions from fossil-fuel burning cement manufacturing and gas-flaring: 1751–2014', http://cdiac.ess-dive.lbl.gov/ftp/ndp030/global.1751_2014.ems.

[10] J. Tyndall, 'On the absorption and radiation of heat by gases and vapours, and on the physical connexion of radiation, absorption, and conduction. The Bakerian Lecture', *Phil. Mag.*, 1861, **22**, 169–94.

[11] S. Arrhenius, 'On the influence of carbonic acid in the air upon the temperature of the ground', *Phil. Mag.*, 1896, **41**, 237–76.

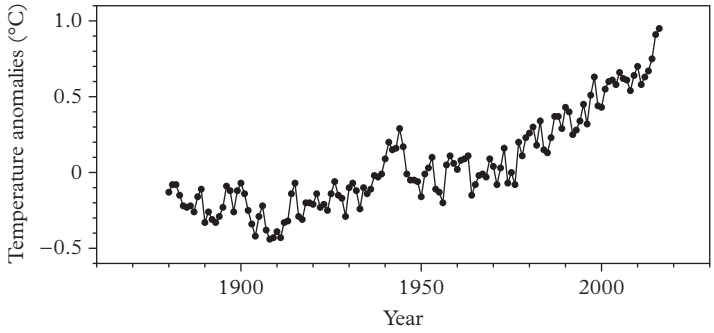

Figure 1.8 *Variations in mean annual atmospheric temperatures compared to the base period of 1901–2000.*

2.3–3 times its level at the time of his writing. That would translate as a change from 295 to 740–890 ppm.

A lengthy debate has transpired since then about the degree to which changes have been due to natural variations or human activity. Improved experimentation and understanding of the interactions between atmosphere, hydrosphere, and biosphere have aided discrimination between contributions, and the bulk of studies and analyses indicate that, qualitatively at least, Arrhenius was onto something. Radiocarbon dating has allowed the characterization of the exchange rates between the atmosphere and oceans, and this resulted in the conclusion that most of the CO_2 added to the atmosphere would be absorbed by the oceans.[12] Hence evidence for trends caused by the increase should be sought in both the oceans and atmosphere at the least.

The assessed annual global land and ocean temperatures[13] have shown a general rise and increase in slope as a baseline to fluctuations of a more short-term nature (Fig. 1.8). The CO_2 can have a direct chemical effect. This can be illustrated by the monitoring of the partial pressure of the gas at an ocean monitoring point with the pH in that region (Fig. 1.9). Again there are short-term variations, but there is a trend in the mean of the pH from *c.*8.12 to *c.*8.06, corresponding to an increase in the concentration of H^+ of *c.*15%.[14] Such a change will cause a shift in the equilibrium concentrations of the carbonate anions ($pK_{a2} = 10.239$ at 25 °C and 0 ion strength) (Eq. 1.1).

$$[HCO_3]^- = [CO_3]^{2-} + H^+. \tag{1.1}$$

This in turn will influence the availability of the aragonite form of calcium carbonate, which is crucial for the formation of shells of marine organisms.

[12] R. Revelle and H. E. Suess, 'Carbon dioxide exchange between atmosphere and ocean and the question of an increase of atmospheric CO_2 during the past decades', *Tellus*, 1957, **9**, 18–27.

[13] GISTEMP Team, 2017: GISS Surface Temperature Analysis (GISTEMP). NASA Goddard Institute for Space Studies. Dataset accessed 2017-11-30 at https://data.giss.nasa.gov/gistemp/. J. Hansen, R. Ruedy, M. Sato, and K. Lo, 2010: 'Global surface temperature change', *Rev. Geophys.*, 2010, **48**, RG4004.

[14] J E. Dore, R Lukas, D. W. Sadler, M. J. Church and D. M. Karl, 'Physical and biogeochemical modulation of ocean acidification in the central North Pacific', *Procl. Natl. Acad. Sci.*, 2009, **106**, 12235–40.

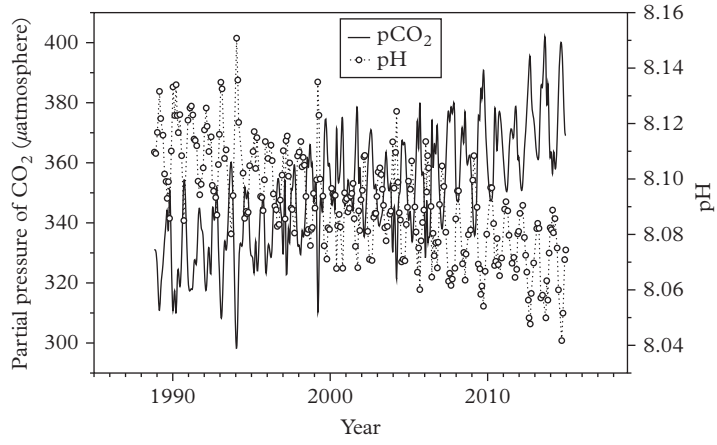

Figure 1.9 *Variations in the seawater CO_2 concentration and pH at Station Aloha near Mauna Loa, Hawaii 1988–2014.*

1.4 Solar Energy Supply

The energy expended using fossil fuels can be set against that supplied by the Sun. This is complicated by the plethora of units used in different communities, so a set of energy definitions is collected in Table 1.1. These relate to materials and processes, and are often described in practical units of energy: kWh or barrels of oil equivalents (BOE). The margin note shows that roughly $\frac{1}{3}$ of the energy consumed in the world is from electricity installations.[15]

[15] World power demand (avg.) 15 TW. Installed electricity capacity 4.5 TW.

The estimate of the solar power received on an imaginary plane normal to the Sun's rays at the edge of the upper atmosphere of Earth averages at 1,367 W m^{-2} (called the solar constant). The maximum value of this is on January 1 when the Earth's elliptical orbit brings it closest to the Sun (by 7%). This impinges upon the Earth as a disc of radius 6,370 km, providing a total input of 1.74×10^{17} W, or 174 PW (petawatts). Spread over the whole surface of the Earth, this affords 342 W m^{-2}, on average (684 W m^{-2} in the day). It is worth noting that the average power demand is 15 TW (terawatts), or less than 10^{-4} of that impinging onto the Earth.

Overall the losses through the atmospheric are described with an **air mass factor** (AM), the ratio of the path length travelled through the atmosphere compared with its depth (Eq. 1.2). The thickness of the most dense region, the **troposphere**, is considerably less at the poles than at the equator (Table 1.2). At the outside of the atmosphere, $AM = 0$. When the Sun is overhead then $\theta_z = 0$, and $AM = 1$. At an incident angle of 60°, $AM = 2$. For solar panel design, an air mass factor of 1.5 is used, corresponding to $\theta_z = 48.2°$. The reduction in

Table 1.1 *Energy definitions and conversions.*

Energy return on investment (EROI)	output/input
Embodied energy of a material	MJ kg^{-1}
Energy content	J kg^{-1}
Energy density	J L^{-1}
Energy concentration	J m^{-2}
Energy efficiency	J/J
Power density	W m^{-2}
Energy intensity	J/$
Tonne of oil equivalent (TOE)	42 GJ
Barrel of oil (*c*.159 L) equivalent (BOE)	6.1 GJ
1eV	8065.7 cm^{-1}
	1.6921×10^{19} J
	96.487 kJ mol^{-1}
1 kWh	3.6 MJ
1 BOE	1694 kWh

Table 1.2 *Height of the troposphere*

At the poles	30,000 ft
At the equator	56,000 ft

Table 1.3 *Solar radiation reaching the surface*

AM value	Proportion	Range (%)
1	0.72	15
1.5	0.64	20
2	0.56	30

solar radiation is not straightforward and depends upon atmospheric conditions (Table 1.3), but at intermediate latitudes the daytime value of 684 W m^{-2} will be reduced to *c*.438 W m^{-2}, which will have a diurnal variation

$$\mathrm{AM} = \frac{\text{path}}{\text{atmosphere}} = \frac{1}{\cos\theta_z}\,,\ \theta_z < 70^{\circ}. \tag{1.2}$$

1.5 Solar Radiation Spectrum

The light from the Sun can be modelled as a **black body**. In everyday parlance this sounds odd, but a black body is a theoretical material that has no intrinsic spectroscopic properties other than that due to its temperature; approximations to this would be a red-hot poker and a incandescent light bulb. One of the key early successes of quantum theory was the successful calculation of an emission maximum using Planck's equation (Eq. 1.3) [B_ν = spectral radiance at frequency ν]

$$B_\nu(\nu, T) = \frac{2h\nu^3}{c^2}\frac{1}{e^{\frac{h\nu}{k_B T}} - 1}. \tag{1.3}$$

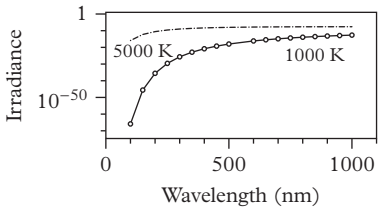

Figure 1.10 *Calculated emission for a black body.*

[16] Laboratory for Atmospheric and Space Physics, University of Colorado, Boulder, Colorado, USA; http://lasp.colorado.edu/home/sorce/instruments/sim/.

As shown in Fig. 1.10, the amplitude of the emission increases greatly with the temperature of the body and also the wavelength of the maximum intensity shortens greatly.

In Wien's law (Eq. 1.4, where $b = 2.8977 \times 10^6$ nm K), the irradiance curves are recognized as having the same shape, and the wavelength of the maximum intensity is inversely rated to the temperature (Fig. 1.11).

$$\lambda_{max} = \frac{b}{T}. \tag{1.4}$$

The energy spectrum of the Sun reaching Earth is measured by the Solar Radiation and Climate Experiment (SORCE), which is a NASA-sponsored satellite mission. One of the spectrometers, SIM (Spectral Irradiance Monitor), has measured the spectrum over the wavelength range 310–2,400 nm (Fig. 1.12), which spans across the irradiance maximum.[16] The energy is mostly in the near

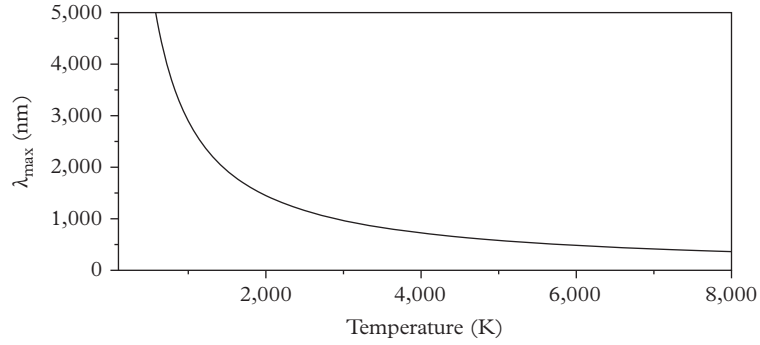

Figure 1.11 *A Wien's law plot of the temperature dependence of the wavelength of maximum intensity for the emission from a black body.*

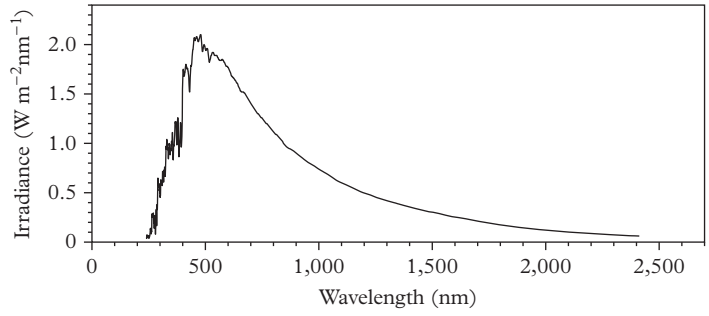

Figure 1.12 *The solar spectrum measured by the SORCE spectrometer SIM at the top of the atmosphere.*

infrared (3,500–700 nm, 51.7%) and the visible (400–700 nm, 38.3%) regions with a minority in the ultra-violet (200–400 nm, 8.7%). The peak radiation is in the visible region (cyan) near 500 nm wavelength, equivalent to a surface temperature of *c*.5,250 °C. The surface regions of the Earth will also afford black body emission. However, the much lower temperatures from those sources will result in much lower intensities and also much longer wavelengths. As shown in Fig. 1.13, the maximum moves from the mid-IR to the far-IR as the temperature is reduced.

The radiation reaching the surface of the Earth is reduced by atmospheric scattering and there are also some specific absorption bands (Fig. 1.14). The strong interactions in the N_2 molecule give a set of **highest occupied molecular orbitals** (HOMOs) of $\pi^4\sigma^2$ which provides the triple bond. There is a large energy gap to the **lowest unoccupied molecular orbitals** (LUMOs), the π^* set. This results in there being no low-lying excited states and it is essentially

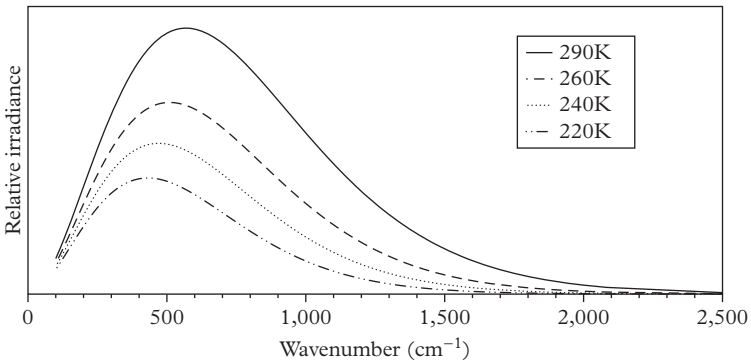

Figure 1.13 *Calculated black body temperatures for temperatures of that at the Earth's surface.*

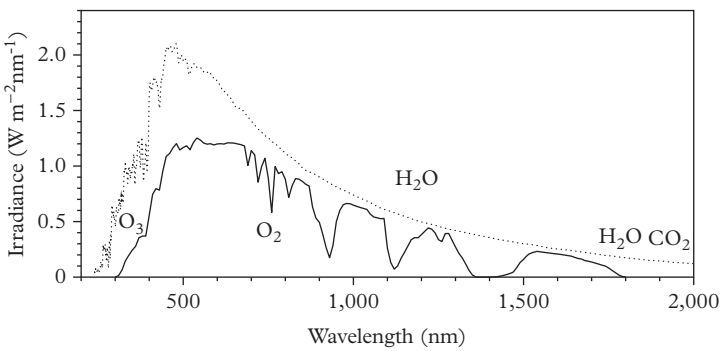

Figure 1.14 *Comparison of the irradiance reaching outer atmosphere (dotted) and at ground level (solid).*

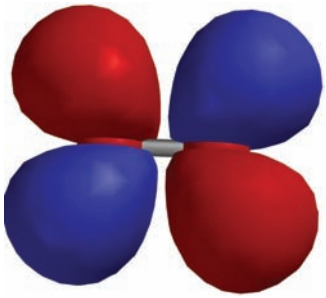

Figure 1.15 *LUMO (π^*) for the beta spins of $^3O_2$.*

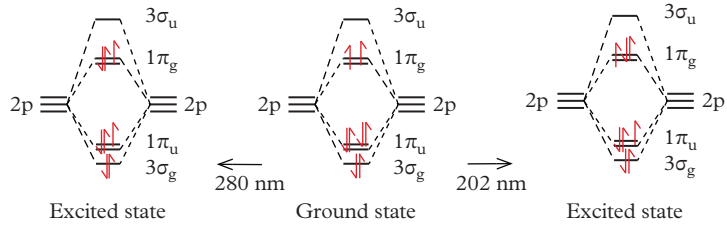

Figure 1.16 *Electronic configurations of the ground state of O_2 ($^3\Sigma^-_g$) and first two spin-allowed transitions (left $^3\Sigma^+_u$, right $^3\Sigma^-_u$).*

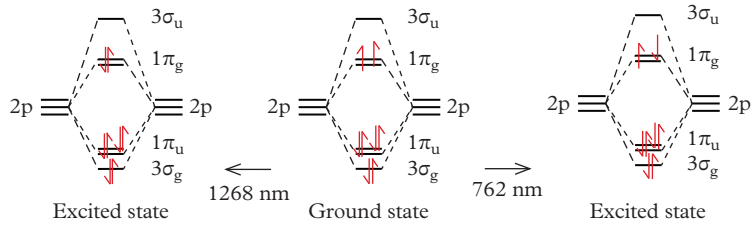

Figure 1.17 *Electronic configurations of the ground state of O_2 ($^3\Sigma^-_g$) and first two spin-forbidden transitions (left $^1\Delta_g$, right $^1\Sigma^+_g$).*

Figure 1.18 *Space-filling model of ozone.*

transparent below an energy of 100,000 cm^{-1} (100 nm). The situation for O_2 is more complicated (Fig. 1.15) and the ground state of the molecule is a spin triplet ($S = 1$)with two unpaired α spins in the π^* orbitals (Fig. 1.16).

The absorptions due to atmospheric oxygen in the UV region arise from very low cross-sections at wavelengths below 270 nm to 200 nm (the Herzberg continuum largely in the stratosphere). These are due to these spin allowed π to π^* transitions of the beta spin electron and associated vibrational fine structure. These are spin-allowed bands; in other words; there is no change in the spin quantum number, S:

$$\Delta S = 0. \tag{1.5}$$

Extension 1.1 *An oddity: liquid oxygen is blue*

One of the characteristics of oxygen is that the liquid is blue in colour, as well as being paramagnetic. The spin-allowed absorption bands in the ultraviolet cannot account for the blue colour, which is expected to result from absorption bands in the red. The electronic configurations of the two lowest-energy spin-forbidden transitions ($\Delta S = -1$ by spin flips within the π^* set) are shown in Fig. 1.17. The lowest-energy absorption from $^3O_2$ to $^1O_2$ is in the near IR (1,268 nm), as is the second transition (762 nm). There are two strong absorptions at 630 and 577 nm which arise from the harmonic of the first excited state (Fig. 1.14). These are much weaker bands than those dominant in the gas phase but do give observable dips in the solar spectrum at the Earth's surface.

In the ultraviolet much of the atmospheric absorption of the solar spectrum is due to electronic transitions in ozone. There is an electronic transition of ozone centred close to 600 nm that gives rise to the Chappuis bands in the troposphere; there are weaker absorptions near 1,000 nm called the Wulff bands. The main effect though is due to the absorption near 260 nm which has a cross-section 10^4 higher than the Wulff bands (called Hartley and Huggins bands). Based on the energy level diagram in Fig. 1.19, the Chappuis transition can be assigned to a spin-allowed transition from the HOMO to a π^* LUMO state (Fig. 1.20); the spin-forbidden transition will give rise to the Wulff bands. The intense bands near 260 nm emanate mainly from the deeper-lying HOMO-2 orbital with π non-bonding character.

At the other end of the irradiance spectrum (Fig. 1.14), above 2500 nm (4000 cm^{-1}), the absorption is due to the stretching modes of water with their associated rotational fine structure. In the near infra red, the absorptions are mainly due to higher harmonics and combination bands of the of the fundamentals found in the mid-infrared region. There are also spin-forbidden transitions to $^1O_2$ states in the visible and NIR (See Extension 1.1).

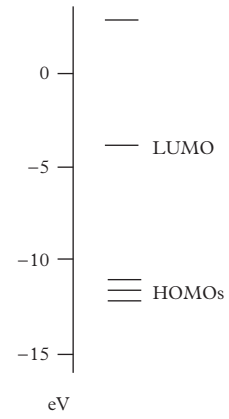

Figure 1.19 *Frontier orbitals of ozone.*

1.6 Absorption of the Energy Emission from Earth

The surface of the Earth itself behaves approximately as a black body, with its spectrum fitting a temperature of 290 K, although the distribution of temperatures will vary with latitude and season. The emission maximum is in the mid infrared

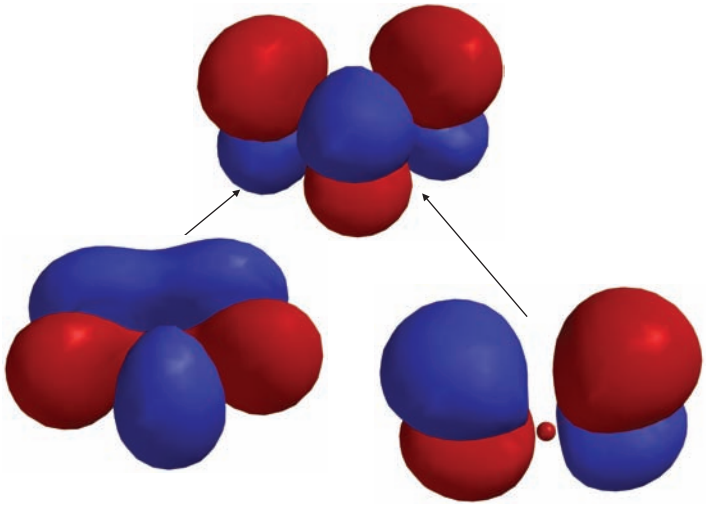

Figure 1.20 *Transitions from the HOMO (left) and HOMO-2 (right) levels to the LUMO (π^*) of O_3.*

near 600 cm^{-1} (Fig 1.13). Above the surface and the boundary layer is the region of the atmosphere called the troposphere. This is the region of most weather events and stretches to about 9 km at the poles and about 17 km at the equator (Table 1.2). Separating that from the **stratosphere** is a region called the **tropopause**. This is a quiet region and movement across the tropopause is relatively small. Hence this can also be considered another black body, with a temperature of 220 K and an emission maximum near 400 cm^{-1} (Fig. 1.13). The measured emission spectra (Fig. 1.21) show maxima following the tracks followed by the black-body curves at 299 and 257 K for tropical and sub-Arctic

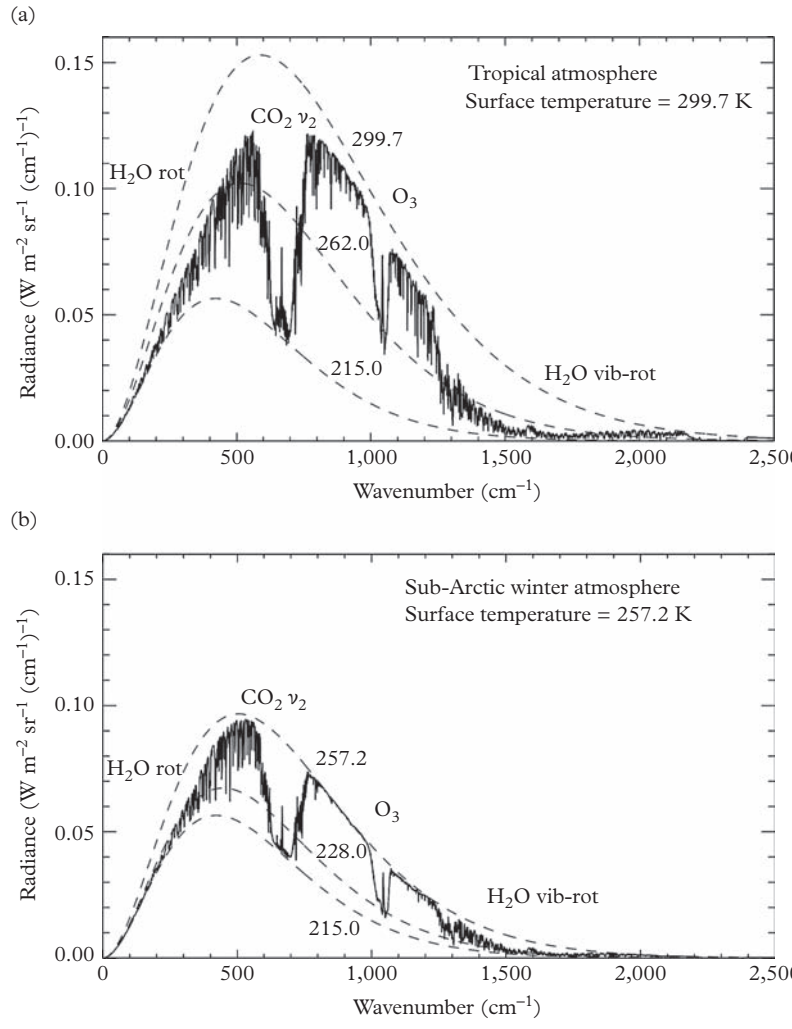

Figure 1.21 *Emission spectra from the Earth measured at the top of the atmosphere for tropical and sub-Arctic winter regions.*

conditions.[17] The curve for the minimum emission tracks that of a black-body at 215 K, taken to be the temperature at the tropopause. The area between those curves represents the energy that could be dissipated by a clear atmosphere if there were no absorbers in the troposphere.

However, this is clearly not the case. In the sub-Arctic region the observed emissions in the 800–900 and 1,100–1,200 cm^{-1} regions of the spectrum are close to that of the Earth's surface, consistent with a virtually transparent troposphere.

However, below 150 cm^{-1} and between 600 and 700 cm^{-1} the emission level is essentially that of the tropopause. In other words, the IR radiation in those regions has been absorbed and retained in the troposphere.

The vast majority of atmosphere components are IR transparent. The third most abundant gas is argon, which being mono-atomic can have no vibrations. The two major components N_2 and O_2 are obviously homonuclear diatomics with a centre of symmetry.[18] Thus their sole vibration creates no dipole change and is IR inactive.

The fundamental energy of a vibration, ν, is dependent upon the reduced mass (μ) of a diatomic molecule with masses m_1 and m_2, and the force constant of the bond (k) (Eq. 1.6):

$$\nu = \frac{1}{2\pi}\sqrt{\frac{k}{\mu}}, \mu = \frac{m_1 m_2}{m_1 + m_2}. \tag{1.6}$$

For a harmonic oscillator, the selection rule is that the quantum number ν provides a single transition energy by

$$\Delta\nu = \pm 1. \tag{1.7}$$

However, the energy profile of a vibration is not symmetrical, flattening out as the interatomic distance approaches the dissociation distance for the bond. This **anharmonicity** allows other transitions to occur:

$$\Delta\nu = \pm 1, \pm 2, \ldots. \tag{1.8}$$

The result of this is a suite of harmonic and combination bands, as was observed in the solar radiance spectra observed on the surface of Earth (Fig 1.14). Absorption due to water and carbon dioxide was evident in regions above 1,100 nm in wavelength (*c.*9,000 cm^{-1}).

The three major contributors to the absorptions are water vapour, CO_2 (Fig. 1.22), and O_3 (Fig. 1.18). This is discussed in more detail in Extension 1.3, but we can assign the molecular motions that are most significant in the absorption of IR radiation (Fig. 1.21). For CO_2, the absorption features near 650 cm^{-1} are due to the bending of CO_2; the complex features at low energy are due to rotations of vapour phase water. Particularly in the tropical regions there is evidently a higher level of water vapour in the troposphere, and in that region the absorption due to the rotational fine structure of gas phase water associated with the bending

[17] J. Harries, B. Carli, R. Rizzi, C. Serio, M. Mlynczak, L. Palchetti, T. Maestri, H. Brindley and G. Masiello, 'The Far-Infrared Earth', *Rev. Geophys.* 2008, **26**, RG4004.

[18] It is helpful in this context that N_2O, NO_2, and NO are endothermic and endoergic (Table 1.4).

Table 1.4 *Formation energies (kJ mol^{-1}).*

NO_x	ΔH^o	ΔG^o
N_2O	81.6	103.8
NO_2	33.9	51.9
NO	90.4	86.6

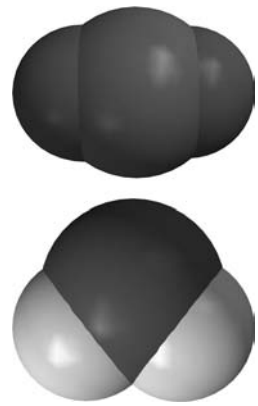

Figure 1.22 *Space-filling models of CO_2 and H_2O.*

[19] J. H. Butler and S. A. Montzka, 'The NOAA Annual Greenhouse Gas Index (AGGI)', 2019 in https://www.esrl.noaa.gov.

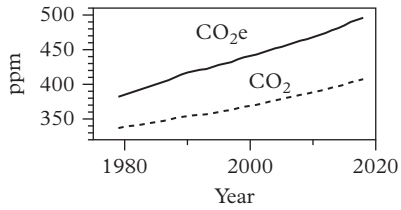

Figure 1.23 *Estimation of the effective concentration of IR absorbing gases as CO_2 equivalents.*

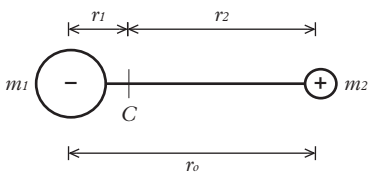

Figure 1.24 *A rigid dipolar diatomic molecule of masses m_1 and m_2 separated by $r_0 = r_1 + r_2$.*

vibration is also apparent. The other obvious feature can be assigned to modes of ozone. These and other gases add to the absorption of energy in the troposphere. Their effects are cumulated relative to CO_2, and thus are represented as CO_2 equivalents (CO_2e). Estimates are available from 1979 (Fig. 1.23).[19] The rate of increase of CO_2e is significantly higher than that of CO_2 alone, indicating that there are other contributors with marked effects.

Water has a permanent dipole moment and so rotation of the molecule will provide a dynamic dipole that can interact with electromagnetic radiation and thus transitions are allowed. This is not the case for the homonuclear diatomics N_2 and O_2, nor for linear CO_2.

If we begin thinking about rotational spectra with a diatomic molecule, we will need to consider a heteronuclear molecule such as HCl or CO, depicted in general in Fig. 1.24. The dipole can be envisaged as rotating about the centre of gravity, C, the position of which will conform to the balance of moments (Eq. 1.9):

$$m_1 r_1 = m_2 r_2 = m_2(r_0 - r_1). \tag{1.9}$$

The moment of inertia, I, is defined by Eq. 1.10:

$$I = m_1 r_1^2 + m_2 r_2^2. \tag{1.10}$$

Using the balance of moments equations, the definition of the moment of inertia can be rewritten in terms of the reduced mass, μ, as Eq. 1.11:

$$I = \frac{m_1 m_2}{m_1 + m_2} r_0^2 = \mu r_0^2. \tag{1.11}$$

The energy of the rotational levels, $\epsilon_{\mathcal{J}}$ in cm^{-1}, has been shown to be Eq. 1.12:

$$\epsilon_{\mathcal{J}} = B\mathcal{J}(\mathcal{J}+1), \mathcal{J} = 0, 1, 2, \ldots. \tag{1.12}$$

where B, the rotational constant, is given by Eq. 1.13:

$$B = \frac{h}{8\pi^2 Ic}. \tag{1.13}$$

The transition energies follow the selection rule (Eq. 1.14):

$$\Delta\mathcal{J} = \pm 1, \tag{1.14}$$

and differ depending upon the $\mathcal{J}$ in question. For example, we can compare the transition energies from 0 and from 1 (Eqs. 1.15, 1.16):

$$\Delta\epsilon_{0\text{-}1} = \epsilon_1 - \epsilon_0 = B(1+1) - 0 = 2B \tag{1.15}$$

$$\Delta\epsilon_{1\text{-}2} = \epsilon_2 - \epsilon_1 = B(2)(2+1) - B(1+1) = 4B. \tag{1.16}$$

Rotational splittings are comparable to, or less than, the Boltzmann energy under atmospheric conditions and so there will be significant populations of a number of ground states, giving rise to a sequence of lines separated by $2B$. These series will be sensitive to isotopic substitution due to the relationship between energy and the moment of inertia. As an example, we compare $^{1}H^{35}Cl$ (B_1) with $^{2}H^{35}Cl$ (B_2) (Eq. 1.17):

$$\frac{B_1}{B_2} = \frac{I_2}{I_1} = \frac{\mu_2}{\mu_1} = \frac{(2)(35)(1+35)}{(1)(35)(2+35)} = \frac{(2)(36)}{(1)(37)} = 1.94. \tag{1.17}$$

Hence the spectra of atmospheric gases will include sequences for the isotopomers. This also shows that the spacing between the rotational lines will tend to reduce with increasing mass. That leaves water displaying a rotational spectrum over a very wide energy range.

The complexity of the spectra increases with less symmetrical structures. The linear molecule HCl has two rotational degrees of freedom, but they are degenerate and can be defined by one rotational constant. For non-linear, pyramidal molecules like ammonia (NH_3), or CFC-11 ($CFCl_3$), there are three rotational degrees of freedom. The threefold axis of symmetry (labelled z or the parallel axis, $\|$) contains one axis and also means that two of the Cartesian axes (x and y, the perpendicular axes, $\perp$) are rendered equivalent. This is called a **symmetric-top** molecule, which needs two moments of inertia to describe the rigid shape, each with its own quantum number to relate the energy levels (Eq. 1.18).

$$\epsilon_{\mathcal{J},K} = B\mathcal{J}(\mathcal{J}+1) + (A-B)K^2, \mathcal{J} = 0, 1, 2, \ldots K = \mathcal{J}, \mathcal{J}-1 \ldots -\mathcal{J}, \tag{1.18}$$

where B and A are the rotational constants given by Eq. 1.19:

$$B = \frac{h}{8\pi^2 I_\perp c}, A = \frac{h}{8\pi^2 I_\| c} \tag{1.19}$$

and the selection rules is (Eq. 1.20):

$$\Delta\mathcal{J} = \pm 1, \Delta K = 0. \tag{1.20}$$

From these relationships the transition energies can be calculated (Eq. 1.21). The spectrum is shown to be independent of the rotation about the z-axis (the $\|$

axis) since rotation around it will not move the molecule dipole (Eq. 1.22); this is the same as for the rotation about the internuclear axis of the linear molecule.

$$\epsilon_{J+1,K} - \epsilon_{J,K} = [B(\mathcal{J}+2)(\mathcal{J}+1) + (A-B)K^2] - [B\mathcal{J}(\mathcal{J}+1) + (A-B)K^2] \tag{1.21}$$

$$= 2B(\mathcal{J}+1). \tag{1.22}$$

For most other molecules like water, called an **asymmetric top**, the situation is more complex. There will be three rotational degrees of freedom, each with its own moment of inertia. With additional structural complexity, the approximation of a rigid molecule becomes less valid. The motion itself creates molecular distortions.

In the water vapour spectrum the fine structure around 1,600 cm^{-1} can be assigned to the rotational-vibrational structure. The vibrational frequency is labelled the Q branch of the spectrum ($\Delta\mathcal{J} = 0$), and straddling it are the P and R branches where the rotational quantum numbers respectively decrease, giving a lower transition energy, and increase, raising the transition energy from that of the vibration alone. The selection rules for simultaneous vibrations and rotations vary with the shape and symmetry of the molecule and the vibration (Eqs 1.23–1.26):

Diatomic linear molecules:vibrations parallel to the principal axis:

$$\Delta\nu = \pm 1, \Delta\mathcal{J} = \pm 1 (\Delta\mathcal{J} \neq 0). \tag{1.23}$$

Linear molecules: vibrations perpendicular to the principal axis:

$$\Delta\nu = \pm 1, \Delta\mathcal{J} = 0, \pm 1. \tag{1.24}$$

Symmetric-top molecules: parallel vibrations:

$$\Delta\nu = \pm 1, \Delta\mathcal{J} = 0, \pm 1, \Delta K = 0. \tag{1.25}$$

Symmetric-top molecules: perpendicular vibrations:

$$\Delta\nu = \pm 1, \Delta\mathcal{J} = 0, \pm 1, \Delta K = \pm 1. \tag{1.26}$$

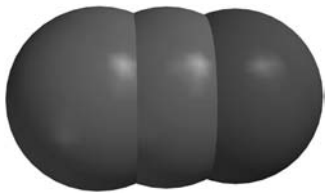

Figure 1.25 *Space-filling model of N_2O.*

In all cases, including the anharmonicity of the vibration allows $\Delta\nu$ also to take higher integer values. This pattern shows that the rotational fine structure of a linear molecule associated with vibrational modes along the molecular axis will have no Q branch. All other modes (Fig. 1.25) will, including the bending modes of linear molecules like CO_2 and N_2O. The perpendicular vibrational modes of symmetric-top molecules will be further complicated with series of rotational transitions based on the moments of inertia both $\parallel$ and $\perp$ to the principal axis.

Extension 1.2 *Beyond the model of the rigid rotor*

The treatment used so far for rotational transitions has inbuilt inconsistencies. One of these is that we have assumed that there is no change in the bond length during a rotation and even when the motion is combined with a vibration. In reality vibrations occur hundreds of times within the timescale of a molecular rotation, and so the bond length does undergo change, and this will affect the value of the rotational constant (Eq. 1.27). Also, there is a centrifugal effect so that the higher the rotational level, the greater the tendency to increase the bond length. As a result, the rotational spectrum of, for example, a diatomic molecule will show a decrease in line separation and that decrease will increase with $\mathcal{J}$ *values.*

$$B \propto \frac{1}{r_o^2}. \tag{1.27}$$

This effect can be accounted for with a centrifugal distortion constant, D (Eq. 1.28), amounting to a contribution for diatomics of $< 0.01\ cm^{-1}$. *Hence in the rotational-vibrational spectrum, which may be recorded at the order of c.1,000* cm^{-1}, *this effect is small.*

$$\epsilon_{\mathcal{J}+1} - \epsilon_{\mathcal{J}} = 2B\mathcal{J}(\mathcal{J}+1) - 4D(\mathcal{J}+1)^3. \tag{1.28}$$

However, the effect of the change in the equilibrium interatomic distance of a diatomic with vibrational level is significant. The energy required to effect the ro-vibrational transition, the band origin or centre, is of energy $\bar{\omega}_e$ *(Eq. 1.29). Anharmonicity provides a shift to lower energy by the factor* x_e; *then the energy of the transitions (Eq. 1.30) is further modified by the rotational constant, B, and quantum numbers,* $\mathcal{J}$, *of the vibrational ground state (*$\mathcal{J}''$*) and vibrational excited state (*$\mathcal{J}'$*) (Eq. 1.29). For* $v = 0$ *to 1, this corresponds to Eq. 1.31.*

$$\epsilon_v = \left(v + \frac{1}{2}\right)\bar{\omega}_e - \left(v + \frac{1}{2}\right)^2 \bar{\omega}_e x_e \tag{1.29}$$

$$\Delta\epsilon_{\mathcal{J},v} = \epsilon_{\mathcal{J}',v=1} - \epsilon_{\mathcal{J}'',v=0} \tag{1.30}$$

$$\Delta\epsilon_{\mathcal{J},v} = \bar{\omega}_e(1 - 2x_e) + B(\mathcal{J}' - \mathcal{J}'')(\mathcal{J}' + \mathcal{J}'' + 1)cm^{-1}. \tag{1.31}$$

So far we have considered the vibrational and rotational energies as coming from independent factors—called the ***Born–Oppenheimer approximation****. But we have accepted that the bond length, and hence the rotational constant, will be affected by the vibrational energy level (Eq. 1.32):*

$$B_v = B_e - \alpha\left(v + \frac{1}{2}\right). \tag{1.32}$$

Taking this together, we can amend Eq. 1.31 to include the break-down of the Born–Oppenheimer approximation (Eq. 1.33):

$$\Delta\epsilon_{\mathcal{J},v} = \bar{\omega}_e(1 - 2x_e) + B_1\mathcal{J}'(\mathcal{J}'+1) - B_o\mathcal{J}''(\mathcal{J}''+1)cm^{-1}. \tag{1.33}$$

Both anharmonicity and the effect of vibrational energy level on the rotational constant mean that the higher-level transitions become less separated in energy.

Extension 1.3 *The IR absorptions of triatomic molecules*

Four key triatomic molecules in the troposphere are CO_2, O_3, N_2O, and H_2O (Fig. 1.26). CO_2 is linear and centrosymmetric (point group $D_{\infty h}$). Of the nine (3N) degrees of freedom of the triatomic, there are three resulting in translations and two to rotations (the rotation around the interatomic axis is not a valid motion). The remaining four (3N-5) motions comprise two stretching vibrations and two rotations. The symmetric stretch results in no dipole moment change and thus is IR inactive. The antisymmetric stretch is of relatively high energy (2,345 cm^{-1}) compared to the emission spectrum of the surface of the Earth. The bending vibration is doubly degenerate and occurs around 667 cm^{-1}, close to the maximum black-body surface emission.

N_2O is linear and non-centrosymmetic (Point group $C_{\infty v}$). As for carbon dioxide, there are two stretching vibrations and a doubly degenerate pair of rotational modes. Again, the antisymmetric stretch is high in energy (2,224 cm^{-1}), but in this case the symmetric stretch is a very strong allowed IR absorption and has an energy within the sensitive region (1,285 cm^{-1}). The bending vibration occurs around 589 cm^{-1}, also close to the maximum black-body surface emission.

O_3 is non-linear (Point group C_{2v}), and has a third viable rotation axis, leaving three (3N-6) remaining for vibrations: two fundamental stretching modes (1,355 and 1,033 cm^{-1}) and one bend (528 cm^{-1}), all in the sensitive region. All these spectra are

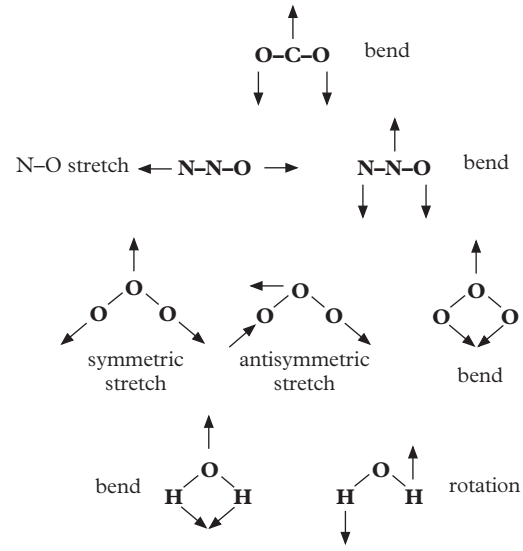

Figure 1.26 *Motions of triatomic molecules that contribute significantly to energy absorption in the troposphere.*

complicated by the presence of isotopes (giving a variety of structural possibilities called isotopomers) by overtone and combination bands to higher energy, and by vibrational-rotational fine structure. Thus the IR spectra provide excellent fingerprints of these gaseous molecules.

H_2O has a structure akin to that of O_3 (Point group C_{2v}), and so the IR fundamentals follow the same pattern. Here the low mass of hydrogen renders the two stretching modes (around 3,700cm^{-1}) to be outside the intense region of the Earth's surface emission. The bending mode (1,595 cm^{-1}) is towards the top of this energy range, but the absorption spectrum is extended greatly by the highly complex vibrational-rotational pattern as well as additional features from the isotopomers. The water molecule has a permanent dipole moment and low-mass atoms. As a result, absorptions due to the pure rotational spectrum are strongly evident below 1,000 cm^{-1}.

The effect of an individual gas on the trapping of energy will be related not only to its concentration, but the intrinsic absorption cross-section of the vibrations and the intensity of the emission of the surface of Earth at the energy of the IR transition. The intensity of an infrared absorption is related to the change in the dipole during the vibration. For stretching vibrations, in which the interatomic distance is changed around the equilibrium bond length, there are two factors which might influence the intensity.

First, a polar bond has a dipole at equilibrium, and so changing the interatomic distance would be expected to change the dynamic dipole (Fig. 1.27). The stretching of a polar bond would change the separation between the partial charges. It may also reduce the covalency and thus tend to localize more charge.

In a second type of effect, the degree of π bonding in a heteronuclear bond can change during the travel of a stretching mode, and this can also change the dipole. This can be illustrated using resonance forms of CO_2 and N_2O (Fig. 1.28). The asymmetric stretch in CO_2 would tend towards the right-hand resonance form with a large induced dipole. Accordingly, the intensity of this mode in the IR is very strong. But the relatively high energy of this vibration means that its contribution to IR energy storage is not as high as it might be. Stretching of the N–O bond would reduce the N–O π bonding, which will also induce an increased dipole for that bond and change the overall molecular dipole. This band is much closer in energy to the maximum for energy emission from the surface of the Earth.

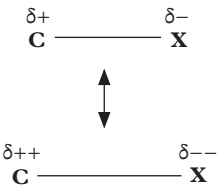

Figure 1.27 *A dynamic dipole from interatomic distance changes.*

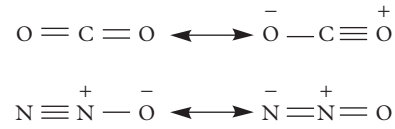

Figure 1.28 *Resonance forms of CO_2 and N_2O showing how a dynamic dipole arises from interatomic distance changes.*

Extension 1.4 *The IR absorptions of five-atom molecules*

There are four C-X bonds and six X-C-X angles in a tetrahedron, one more than the number of degrees of freedom. It is impossible to increase or decrease all the angles simultaneously as would happen in a symmetric bend, hence only five bending modes are valid. To be IR active a vibrational mode must have the same symmetry as a Cartesian axis. The point group of CH_4 is T_d and x, y, and z all fall within the triply degenerate t_2 representation. The antisymmetric stretches and a set of bending modes